Title	A 1/f noise upconversion reduction technique applied to class-D and class-F oscillators
Authors(s)	Shahmohammadi, Mina; Babaie, Masoud; Staszewski, Robert Bogdan
Publication date	2015-02-26
Publication information	Proceedings of 2015 IEEE International Solid-State Circuits Conference (ISSCC) 2015
Conference details	2015 IEEE International Solid-State Circuits Conference (ISSCC), San Francisco, California, USA, February, 2015
Publisher	IEEE
Item record/more information	http://hdl.handle.net/10197/7316
Publisher's statement	© © 2015 IEEE. Personal use of this material is permitted. Permission from IEEE must be obtained for all other uses, in any current or future media, including reprinting/republishing this material for advertising or promotional purposes, creating new collective works, for resale or redistribution to servers or lists, or reuse of any copyrighted component of this work in other works.
Publisher's version (DOI)	10.1109/ISSCC.2015.7063117

25.4 A 1/f Noise Upconversion Reduction Technique Applied to Class-D and Class-F Oscillators

Mina Shahmohammadi, Masoud Babaie, Robert Bogdan Staszewski

Delft University of Technology, Delft, The Netherlands

The 1/*f* (flicker) noise up-conversion degrades the close-in spectrum of CMOS RF oscillators. The resulting 1/f³ phase noise (PN) can be an issue in PLLs with a loop bandwidth of <1MHz, which practically implies all cellular phones. Noise filtering [1] and adding resistors in series with gm-devices drain [2] have shown significant reduction of 1/f³ oscillator PN corner. However, the former needs an additional tunable inductor and the latter degrades PN in the 20dB/dec region, especially in low V_{DD} and high current consumption oscillators.

The flicker noise can up-convert via two major phenomena. First, tail current flicker noise can modulate the oscillating waveform amplitude, which can convert to PN through a nonlinear C-V characteristic of varactors and active devices. The second mechanism is the Groszkowski effect [3]: The presence of harmonic components of the active device current can cause a frequency drift of the tank resonance (see Fig. 25.4.1-top). The fundamental drain current I_{H1} flows into R_p (equivalent parallel resistance of the tank), while its 2nd and 3rd harmonic components, I_{H2} and I_{H3}, mainly take the capacitance path due to its lower impedance. Consequently, the reactive energy stored in the inductance and capacitance is perturbed, shifting the oscillation frequency Δω lower to satisfy the resonance condition. This shift is static but any variation in the I_{H2} (or I_{H3}) to I_{H1} ratio due to the 1/f noise can modulate Δω and show itself as the 1/f³ PN, see Fig. 25.4.1(top-left). This phenomenon is clearly visible and now *dominant* in oscillators with the customary tail current source transistor removed, which is the trend in nanoscale CMOS.

Suppose the tank input impedance Z_{in} demonstrates other peaks at the strong harmonics of the fundamental frequency ω_0. These harmonics would mainly flow into their relative equivalent resistance of Z_{in} instead of its capacitive part, as is shown in Fig. 25.4.1-bottom. Consequently, Groszkowski's effect on the 1/f noise up-conversion will reduce significantly. Specifically core transistor flicker noise modulates the 2nd harmonic of oscillator's virtual ground. This modulation generates 2nd harmonic current in the parasitic C_{gs} capacitors and gets injected to the tank. Consequently, the I_{H2} component is usually the main contributor to the frequency shift. In this work we introduce a tank topology that effectively traps I_{H2} in its resistive part without the cost of an extra area. The tank derives this characteristic from the different behavior of inductors and transformers in differential (DM) and common mode (CM) excitations.

Fig. 25.4.2 shows a 2-turn inductor in DM and CM excitations. In DM, the currents in each turn are in the same direction resulting in an additive flux, while in CM, the opposite currents cancel each other's magnetic flux. Due to this cancellation, the effective CM inductance is very low. The "F_2 inductor" is designed with appropriate spacing between the windings and demonstrates a 4x smaller effective inductance for CM inputs than for DM inputs. The CM input signals cannot see the differential capacitances, hence to be able to set a CM resonance, the capacitors across the tank have to be single-ended. The input impedance of the F_2 tank, Z_{in}, demonstrates two resonant frequencies, $\omega_{DM}=\omega_0$, and $\omega_{CM}=2\omega_0$. The precise inductor geometry controlled by lithography maintains $L_{DM}/L_{CM}\approx4$ and hence $\omega_{CM}/\omega_{DM}\approx2$ over the full tuning range, TR. The lower and broader CM impedance, compared to that of DM, guarantees the 2nd harmonic current flowing mainly to the additional resistive part, even if CM resonant frequency is mis-tuned by 10%.

Fig. 25.4.3 shows a 1:2 turns transformer excited by DM and CM input signals at its primary. In DM excitation, the induced currents at the secondary circulate in the same direction leading to a strong coupling factor, k_m. On the other hand, in CM excitation, the induced currents cancel each other, resulting in a weak k_m. The "$F_{2,3}$ tank" employs the $F_{2,3}$ transformer, single-ended primary and differential secondary capacitors. This tank has two DM and one CM resonant frequencies. For resistive traps at 2nd and 3rd harmonics, $\omega_{CM}=2\omega_{0,DM}$ and $\omega_{1,DM}=3\omega_{0,DM}$, resulting in $L_sC_s=3L_pC_p$ and $k_m=0.72$ [4]. In reality, $L_{pc}>L_{pd}$ due to the metal track inductance L_T connecting the center tap to the supply, thus lower k_m is needed to satisfy both F_2 and F_3 operations. Unlike the F_2 tank, in the $F_{2,3}$ tank, the $\omega_{CM}/\omega_{0,DM}$ and $\omega_{1,DM}/\omega_{0,DM}$ ratio is no longer only dependent on the inductive parts. Careful design of the tunable single-ended primary and differential secondary capacitor banks maintain $\omega_{CM}/\omega_{0,DM}\approx2$ and $\omega_{1,DM}/\omega_{0,DM}\approx3$ over the full TR.

To demonstrate how this technique can reduce the flicker noise up-conversion, we employ the F_2-tank to a class-D [5], and $F_{2,3}$-tank to a class-F [4] oscillator. These classes of oscillator are chosen for their strong amount of I_{H2}.

The original class-D oscillator shows promising performance in the 1/f² region but it suffers from the strong 1/f noise up-conversion and frequency supply pushing. All known mitigation techniques (e.g., [6]) seem either ineffective or unsuitable. As shown in Fig. 25.4.4-top, the class-D/F_2 oscillator adopts the F_2 tank. The gm-devices M_1 and M_2 inject a large I_{H2} current into the tank due to the ground-clipping of signals. Fig. 25.4.4 also compares class-D and D/F_2 waveforms. Clearly the rise/fall times are more symmetric in the class-D/F_2 oscillator, which translates to lower DC value of gm-transistors' ISF function and thus lower the 1/f noise up-conversion. The class-D oscillator shows 0.8~2.5MHz 1/f³ corner frequency. A version of class-D with a tail filter [6] was also designed in [5]. A resonator at $2\omega_0$ is interposed between the common source of the transistors and ground. This method is only partially effective, lowering 1/f³ PN corner to 0.6~1MHz, since it only linearizes the gm device and partially reduces the I_{H2} amount. Our method traps I_{H2} in the tank and simulations predict the 1/f³ PN corner of <50 kHz.

The class-F_3 oscillator has a pseudo square-wave oscillation waveform by designing $\omega_{1,DM}=3\omega_{0,DM}$, and avoiding filtering of I_{H3} in the tank. The special ISF function of square waveform oscillation leads to a better PN performance. Simulations show that in this oscillator I_{H2} can be as high as I_{H3}. The class-$F_{2,3}$ oscillator replaces the class-F_3 tank with the $F_{2,3}$ one, as shown in Fig. 25.4.4-bottom. Simulations show that the pseudo square wave of class-F is preserved and the 1/f³ PN corner can be reduced from 300~700 kHz to <30 kHz.

The class-D/F_2 oscillator was prototyped in 40 nm 1P8M CMOS process *without* ultra-thick metal layers. The chip micrograph is shown in Fig. 25.4.7-left. The tank employs a 1.5nH inductor with simulated Q-factor of 12 at 3GHz. $M_{1,2}$ are (200/0.04)μm low-V_t devices which guarantee start-up and class-D operation over PVT. The oscillator is tunable between 3.3–4.5GHz (31% TR) with a 6-bit MOM capacitor bank. Fig. 25.4.5-top shows the PN plots at f_{max} and f_{min} oscillation frequencies, with V_{DD}=0.5V. The 1/f³ PN corner is ~100 kHz at f_{max} and reduces to 60 kHz when all switches are on at f_{min}.

The class-$F_{2,3}$ oscillator was prototyped in 40 nm 1P7M CMOS process *with* an ultra-thick metal layer (see Fig. 25.4.7-right). The tank primary and secondary are 0.58nH and 1.5nH, respectively, and k_m=0.67. The simulated Q-factor of the primary and secondary windings are 13 and 19 at 5GHz. $M_{1,2}$ are (64/0.27)μm thick oxide devices to tolerate large gate voltage swings. The oscillator is tunable between 5.4–7 GHz (25% TR) with two 6-bit MOM capacitor banks. Fig. 25.4.5-bottom shows the PN plots at f_{max} and f_{min} oscillation frequencies, with V_{DD} of 1V. The 1/f³ PN corner is ~130 kHz at f_{max} and reduces to 60 kHz when all switches are on at f_{min}.

In both oscillators the PN in the 1/f² region fits well with the simulations. However, the 1/f³ PN corner is at least ~2x higher than expected mainly due to a $2\omega_0$ disturbance on the supply rail created by the oscillator output buffer. Fig. 25.4.6 summarizes the oscillators' performance and compares them with their counterpart reference designs. Even with the performance degradation due to the unavoidable supply sharing, this technique demonstrates >10–15x improvement in the 1/f³ PN corner in class-D and 5x improvement in class-F with no extra area penalty. It also significantly improves supply pushing.

Acknowledgment:

We thank RF Dept. of HiSilicon and EU ERC Starting Grant 307624.

References:

[1] A. Ismail and A. A. Abidi, "CMOS differential LC oscillator with suppressed up-converted flicker noise," IEEE ISSCC, 2003, pp. 98–99.

[2] S. Levantino, et al., "Suppression of flicker noise up-conversion in a 65nm CMOS VCO in the 3.0-to-3.6GHz band," Proc. ISSCC, 2010, pp. 50–51.

[3] J. Groszkowski, "The impedance of frequency variation and harmonic content, and the problem of constant-frequency oscillator," *Proc. IRE*, vol. 21, pp. 958–981, 1933.

[4] M. Babaie *et al.*, "A class-F CMOS oscillator," *IEEE* JSSC, vol. 48, no12, pp. 3120-3133, Dec. 2013.

[5 L. Fanori *et al.,* "Class-D CMOS oscillators," *IEEE JSSC*, vol. 48, no.12, pp. 3105–3119, Dec. 2013.

[6] E. Hegazi *et al.*, "A filtering technique to lower LC oscillator phase noise," *IEEE JSSC*, vol. 36, no. 12, pp. 1921–1930, Dec. 2001.

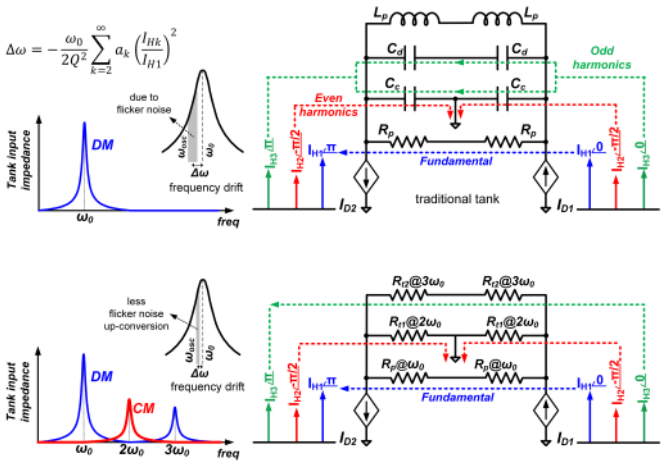

Figure 25.4.1: Current harmonic paths and frequency drift.

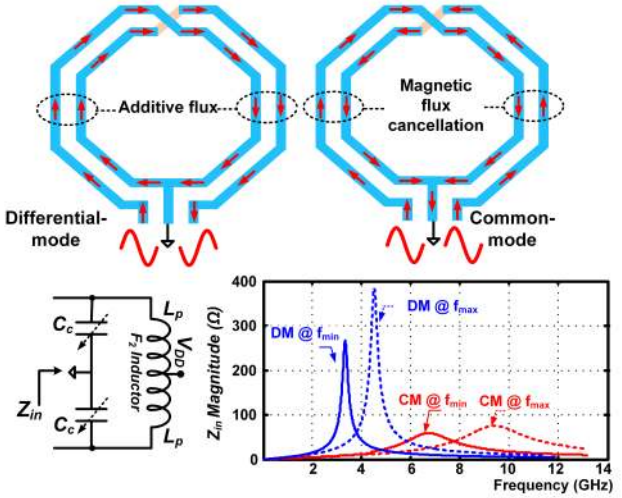

Figure 25.4.2: F_2 inductor, F_2 tank and tank's input impedance.

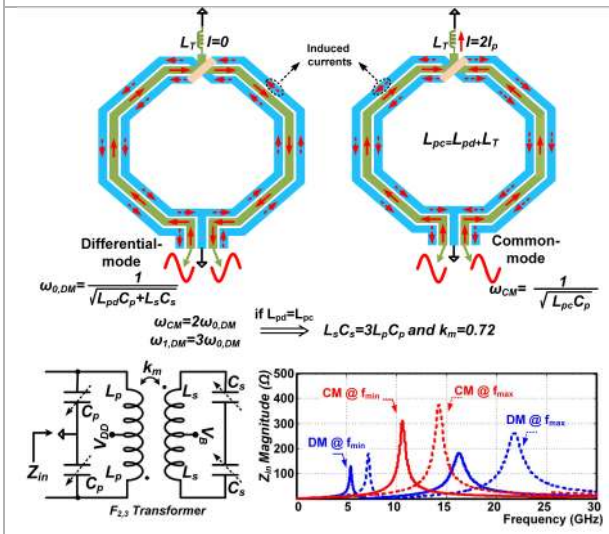

Figure 25.4.3: $F_{2,3}$ transformer, $F_{2,3}$ tank and tank's input impedance.

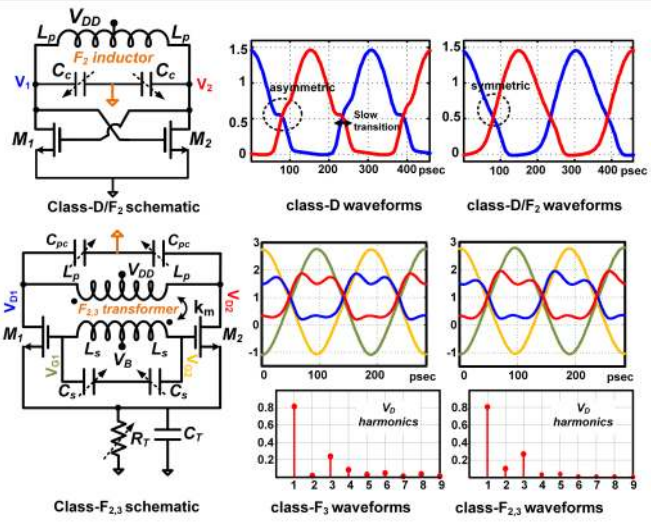

Figure 25.4.4: Oscillators' schematics and waveforms.

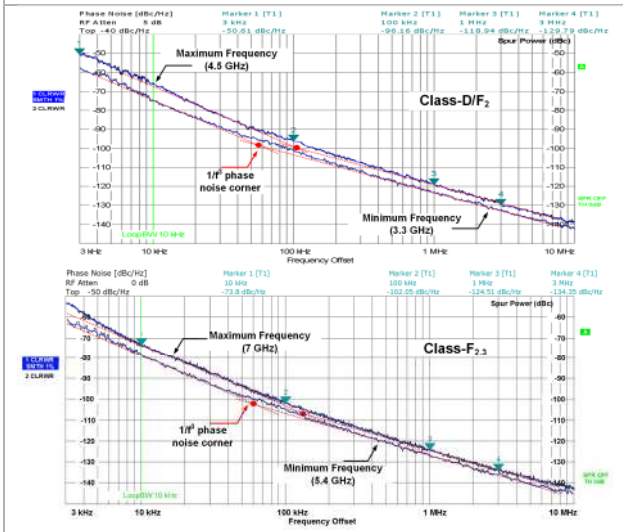

Figure 25.4.5: Oscillators' measured PN.

		Class-D/F_2		Class-D [5]		Noise Filtering Class-D [5]		Class-$F_{2,3}$		Class-F_2[4]
Technology		40 nm		65 nm		65 nm		40 nm		65 nm
Thick metal		No		Yes		Yes		Yes		Yes
V_{DD} (V)		0.5		0.4		0.4		1		1.25
Tuning range (%)		31		45		45		25%		25%
OSC core area		0.1 mm²		0.12 mm²		0.15 mm²		0.13 mm²		0.12mm²
Freq. (GHz)		f_{min} 3.3	f_{max} 4.5	f_{min} 3	f_{max} 4.8	f_{min} 3	f_{max} 4.8	f_{min} 5.4	f_{max} 7	f_{max} 7.4
P_{DC} (mW)		4.1	2.5	6.6	4	6.6	3.6	12	10	15
PN (dBc /Hz)	100kHz	-101.2	-96.2	-101	-91	-102	-92.5	105.3	102.05	-98.5
	1MHz	-123.4	-119	-127	-119	-128	-121	126.7	124.5	-125
	10MHz	-143.4	-139	-149.5	-143.5	-150	-144.5	146.7	144.5	-147
FoM† (dB)	100kHz	185.4	185.3	182.2	178.6	183.2	180.56	189.1	188.9	184.1
	1MHz	187.6	188	188.2	186.6	189.2	189.06	190.5	191.4	190.6
	10MHz	187.6	188	190.7	191.1	191.2	192.56	190.5	191.4	192.6
1/f³ corner (kHz)		60	100	800	2100	650	1500	60	130	700
Freq. pushing (MHz/V)		40 @0.5V	60 @0.5V	140 @0.5V	480 @0.5V	90 @0.5V	390 @0.5V	12 @1V	23 @1V	50 @1.25V

†FOM= $|PN|+20\log_{10}(\omega_0/\Delta\omega)-10\log_{10}(P_{DC}/1mW)$

Figure 25.4.6: Comparison with relevant oscillators.

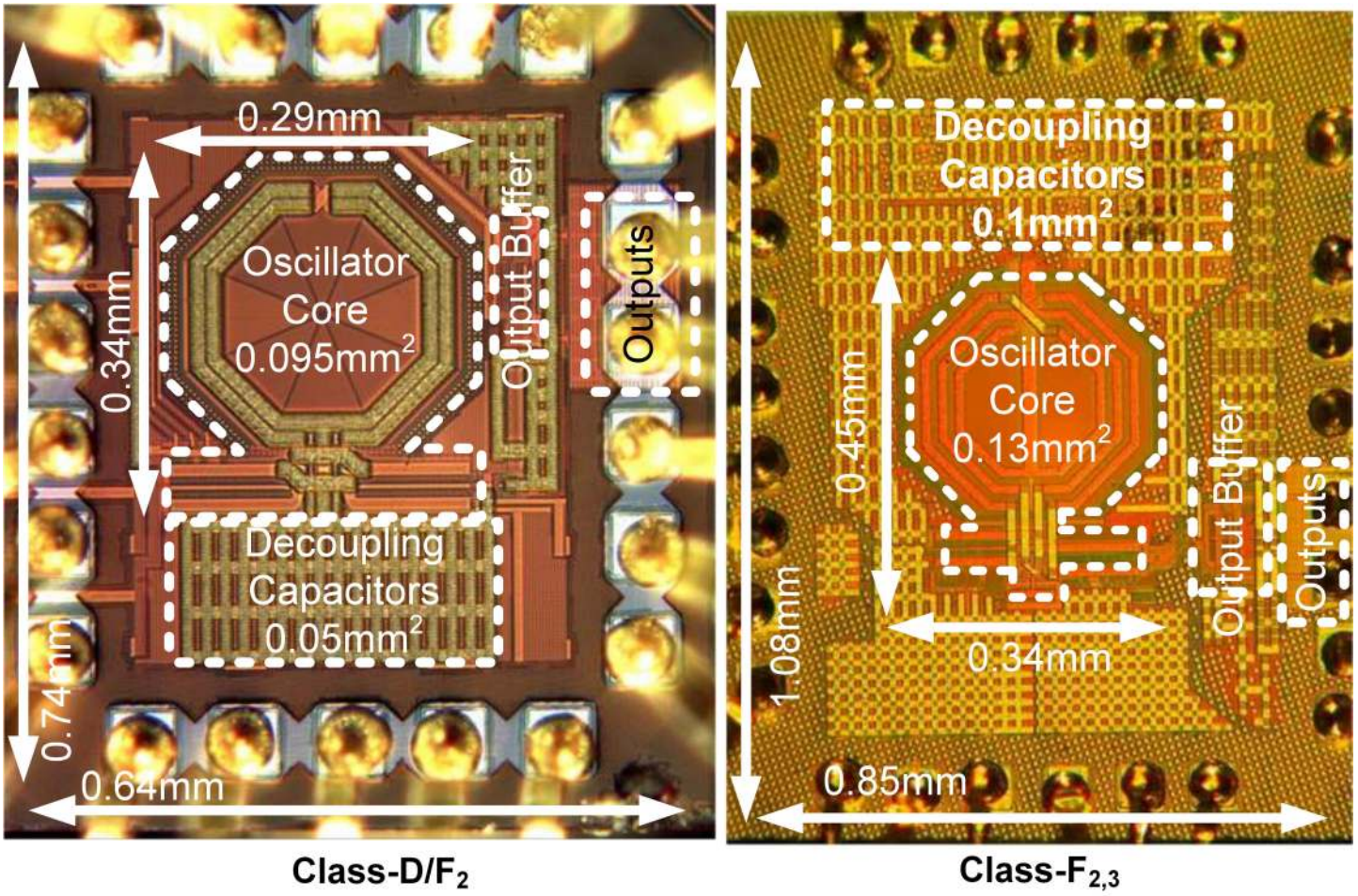

Figure 25.4.7: Oscillators' chip micrograph.